Supporting Information for: Ultrafast triggering of insulator-metal transition in two-dimensional VSe_2

Deepnarayan Biswas,[1] Alfred J. H. Jones,[1] Paulina Majchrzak,[1,2] Byoung Ki Choi,[3] Tsung-Han Lee,[4] Klara Volckaert,[1] Jiagui Feng,[5,6] Igor Marković,[5,7] Federico Andreatta,[1] Chang-Jong Kang,[4] Hyuk Jin Kim,[3] In Hak Lee,[3] Chris Jozwiak,[8] Eli Rotenberg,[8] Aaron Bostwick,[8] Charlotte E. Sanders,[2] Yu Zhang,[2] Gabriel Karras,[2] Richard T. Chapman,[2] Adam S. Wyatt,[2] Emma Springate,[2] Jill A. Miwa,[1] Philip Hofmann,[1] Phil D. C. King,[5] Young Jun Chang,[3,9] Nicola Lanata,[1,10] and Søren Ulstrup[1,*]

[1]*Department of Physics and Astronomy, Interdisciplinary Nanoscience Center, Aarhus University, 8000 Aarhus C, Denmark*

[2]*Central Laser Facility, STFC Rutherford Appleton Laboratory, Harwell 0X11 0QX, UK*

[3]*Department of Physics, University of Seoul, Seoul 02504, Republic of Korea*

[4]*Department of Physics and Astronomy, Rutgers University, Piscataway, NJ 08856, USA*

[5]*SUPA, School of Physics and Astronomy, University of St Andrews, St Andrews KY16 9SS, UK*

[6]*Suzhou Institute of Nano-Tech. and Nanobionics (SINANO), CAS, 398 Ruoshui Road, SEID, SIP, Suzhou, 215123, China*

[7]*Max Planck Institute for Chemical Physics of Solids, Nöthnitzer Straße 40, 01187 Dresden, Germany*

[8]*Advanced Light Source, E. O. Lawrence Berkeley National Laboratory, Berkeley, CA 94720, USA*

[9]*Department of Smart Cities, University of Seoul, Seoul, 02504, Republic of Korea*

[10]*Nordita, KTH Royal Institute of Technology and Stockholm University, Roslagstullsbacken 23, 10691 Stockholm, Sweden*

Supplementary Section 1: Form of the self energy in ARPES simulations

The following mathematical form of the self energy was utilized in our simulations for interpreting the ARPES data, within an energy window of ~0.5 eV from the Fermi level:

$$\Sigma_n(\boldsymbol{k},\omega) = \Sigma_{loc}(\omega) - i\frac{\Gamma}{Z} + \frac{\Delta^2/Z}{\omega + Z(\epsilon_{\boldsymbol{k}n} + \Sigma_0) + i\Gamma_0}\,. \tag{1}$$

Here $\boldsymbol{k}$ is the momentum, ω is the energy, $\epsilon_{\boldsymbol{k}n}$ is a generic band eigenvalue, Γ is scattering rate, Δ is the gap parameter, Γ_0 is a constant related to the change in scattering rate due to Δ and Σ_{loc} is the momentum-independent (local) component of the self-energy:

$$\Sigma_{loc}(\omega) = \Sigma_0 - \frac{1-Z}{Z}\omega\,, \tag{2}$$

which we approximated assuming a linear structure characterized by the quasiparticle residue Z and a constant energy shift Σ_0.

To explain the physical reasons underlying Eq. (1) we note that the corresponding momentum-resolved single-particle Green's function is represented as follows:

$$G_n(\boldsymbol{k},\omega) = \frac{1}{\omega - \epsilon_{\boldsymbol{k}n} - \Sigma_n(\omega,\boldsymbol{k})} = \frac{Z}{\omega - \epsilon^*_{\boldsymbol{k}n} + \Gamma - \frac{\Delta^2}{\omega+\epsilon_{\boldsymbol{k}n}+i\Gamma_0}}\,, \tag{3}$$

where

$$\epsilon^*_{\boldsymbol{k}n} = Z\left(\epsilon_{\boldsymbol{k}n} + \Sigma_0\right). \tag{4}$$

In fact, the last expression in Eq. (3) has the same mathematical structure of the phenomenological self-energy previously used for fitting ARPES data in the presence of a superconducting or charge density wave (CDW) gap [1, 2]. Therefore, in this work, *Eq.* (1) *is designed to represent the CDW effects on a band structure consisting of pre-existing quasi-particle excitations renormalized by electron correlations.*

Note that in Eq. (2) we assumed that $\Sigma_{loc}(\omega)$ acts as a number rather than a matrix. However, in general, the self-energy correction $\Sigma_{loc}(\omega)$ shall be expected to be significant only for the V $3d$ degrees of freedom. Furthermore, considering the symmetry of our system, the d_{z^2}, $d_{x^2+y^2} + d_{xy}$ and $d_{xz} + d_{yz}$ components of the self-energy are not a-priori equal, as they belong to distinct irreducible representations of the point symmetry group of the V atoms. On the other hand, Eq. (2) is a meaningful approximation provided that, for energies ω within ~0.5 eV around the Fermi level, the following hypothesis are verified:

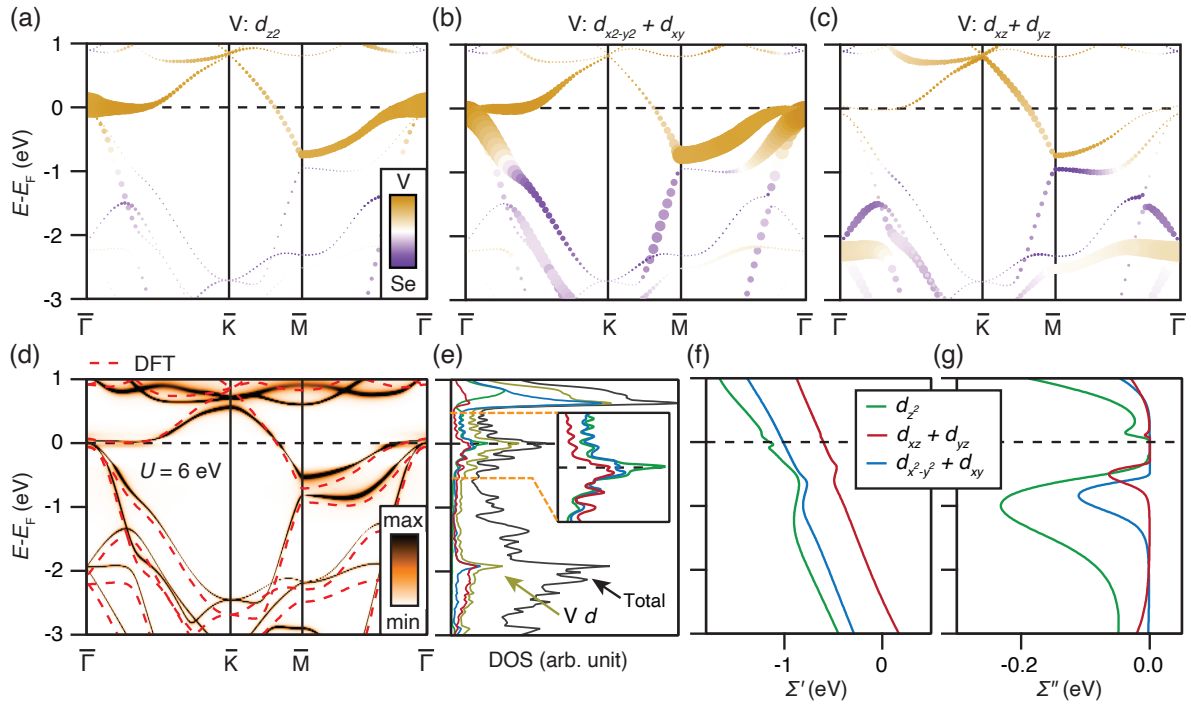

FIG. S1: Theoretical calculations and band character. (a)-(c) DFT calculated bands. The contribution from V and Se atoms are represented by yellow and violet color. The marker size corresponds to the V d_{z^2}, $d_{x^2+y^2}$ + d_{xy} and d_{xz} + d_{yz} orbital characters. (d) LDA + DMFT calculated band structure (U = 6 eV, J = 0.8 eV). The DFT bands are overlayed as red dashed lines. (e) Density of states corresponding to LDA + DMFT calculated band structure, shown in (d). (f)-(g) Energy dependence of the (f) real and (g) imaginary parts of the electronic self energy, respectively.

1) Most of the spectral weight arises from the V 3d electrons.

2) The self-energy is approximately orbital-independent.

3) The momentum-independent local component Σ_{loc} of the self-energy is approximately real and linear with respect to the frequency.

Here we use DFT and LDA+DMFT calculations to prove that these hypotheses are, in fact, approximately applicable to our system. We show the DFT calculated bands resolved with respect to their orbital character in Fig. S1(a)-(c). These calculations indicate that the bands have mostly V 3d character near the Fermi level. Specifically, the spectral weight is dominated by the d_{z^2}, $d_{x^2+y^2}$ + d_{xy} contributions. Fig. S1(d) illustrates the LDA+DMFT band structure obtained for a screened Hubbard interaction strength U = 6 eV and a Hund's

TABLE I: Quasiparticle weights of V $3d$ orbitals for different values of U, at J = 0.8 eV

U	d_{z^2}	$d_{x^2+y^2}$ + d_{xy}	d_{xz} + d_{yz}
5 eV	0.50635	0.78723	0.80550
6 eV	0.49489	0.75884	0.77807
7 eV	0.47736	0.73362	0.75279
8 eV	0.45801	0.70974	0.72878
9 eV	0.43984	0.68810	0.70745

coupling constant J = 0.8 eV. The orbitally-resolved LDA+DMFT local DOS in Fig. S1(e) confirms that, consistent with DFT, most of the spectral weight near the Fermi level has V $3d$ character. Finally, as shown in Fig. S1(f) and (g), the self-energy is approximately linear and similar for all of the V $3d$ orbitals for energies $|\omega| \lesssim 0.5$ eV with respect to the Fermi level. This observation is consistent with the LDA+DMFT quasi-particle weights:

$$Z_\alpha = \left| 1 - \frac{\partial \Sigma'_\alpha}{\partial \omega} \right|^{-1} , \tag{5}$$

see Table 1, which are all $\gtrsim 0.5$, in agreement with our simulation (in the range 0.52 to 0.54).

In Fig. S2 we show the LDA+DMFT bands for three different values of the Hubbard interaction strength U. The bands are found to be very similar for these U values. This indicates that our theoretical predictions are robust.

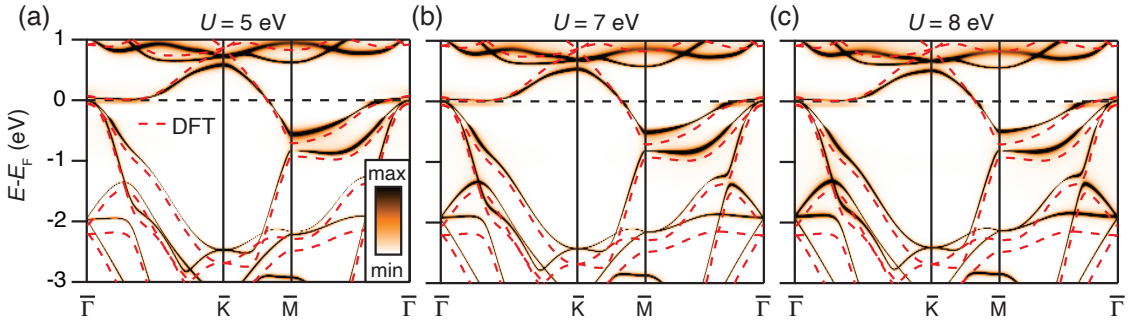

FIG. S2: Behavior of LDA+DMFT bands as a function of U. (a)-(c) LDA+DMFT band structures calculated using the given values of screened on-site Coulomb interaction strength U, at J = 0.8 eV. The bare DFT bands are also shown for comparison (red dashed lines).

Supplementary Section 2: Raw ARPES spectra in metallic and insulating phase

Fig. S3(a) and (b) show static ARPES spectra for both metallic and insulating phases. The dispersion of the top V $3d$ band is different close to k_F due to the formation of the energy gap in the insulating phase. Figure S3(c) presents TR-ARPES snapshots of the spectral changes in these two scenarios before and after optical excitation.

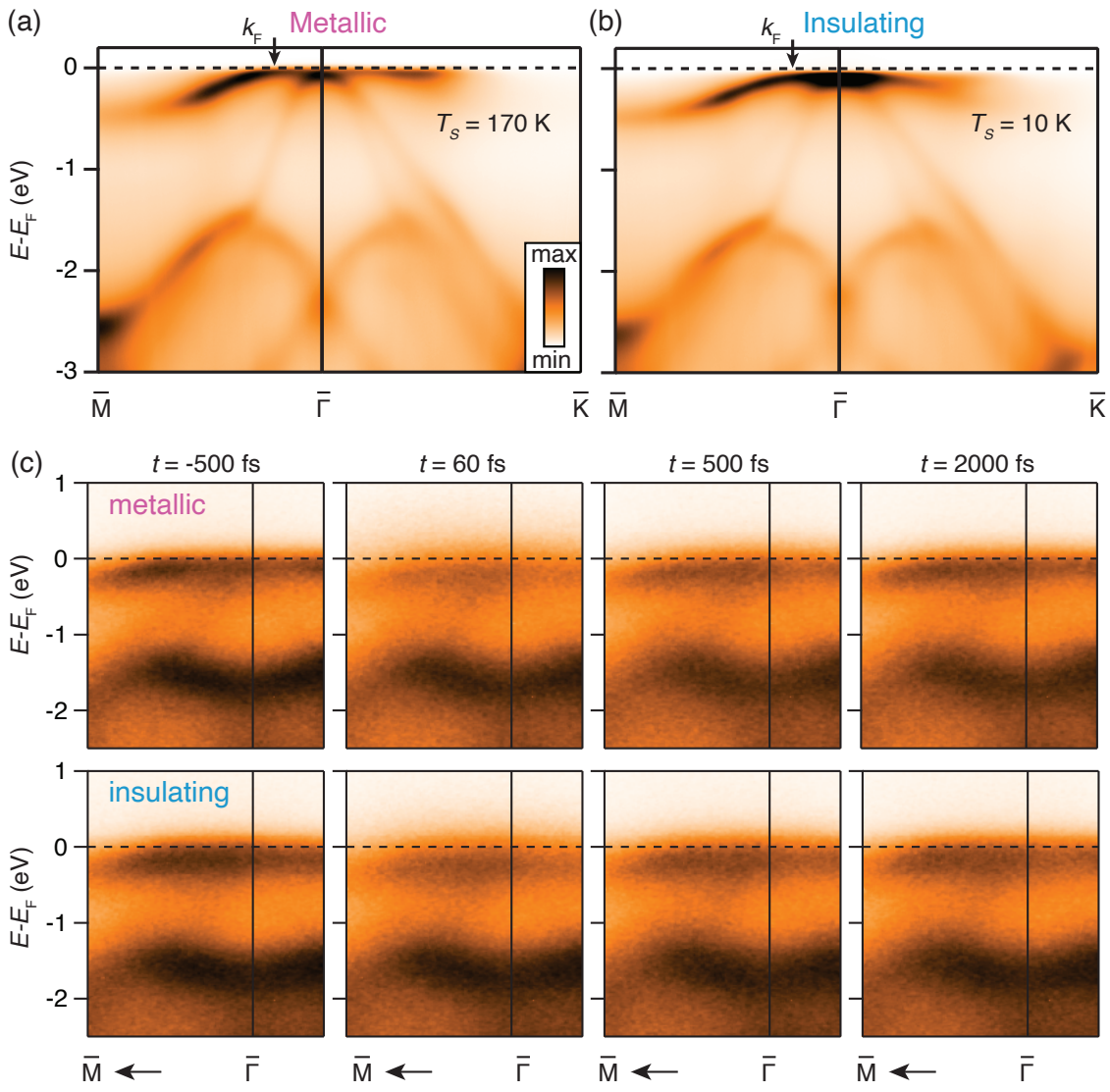

FIG. S3: Comparison of ARPES spectra. (a)-(b) Static ARPES spectra for metallic and insulating phase. (c) TR-ARPES spectra at the given time delays for metallic (top) and insulating (bottom) phase.

Supplementary Section 3: Simulation of ARPES spectra

The ARPES intensity is simulated using the expression

$$\mathcal{I}_{ARPES} = [|\mathcal{M}_n(\boldsymbol{k},\omega)|^2 \mathcal{A}_n(\boldsymbol{k},\omega) n_{\mathrm{FD}}(\omega)] * \mathcal{R}_\omega * \mathcal{R}_k. \quad (6)$$

We expand $\mathcal{M}_n(\boldsymbol{k},\omega)$ in second order polynomial terms of both ω and k [3]. The energy and momentum resolution functions ($\mathcal{R}_\omega$ and $\mathcal{R}_k$) are known from instrument calibration and remain fixed for a given measurement. Furthermore, in static ARPES measurements we use that $T_e = T_s$ and $\mu = E_{\mathrm{F}}$ such that n_{FD} is fully specified. The parameters describing $\mathcal{M}_n(\boldsymbol{k},\omega)$ and $\Sigma_n(\boldsymbol{k},\omega)$ are obtained by performing a 2D fit of a simulated (ω, k)-dependent intensity to the corresponding ARPES spectrum. In static condition, we find that a satisfactory fit is obtained using a quasiparticle residue Z in the range of 0.52 to 0.54. Since the values of Z and Δ at a given T_s are intrinsic properties of the V $3d$ states that are independent of measurement configuration, we apply the values obtained from the static ARPES simulations to describe the TR-ARPES spectra. Note that the Se $4p$ states at higher binding energies are well-described by the DFT bands and using a scattering rate that is merely expressed in terms of first order polynomials of ω and k. The parameters describing $\mathcal{M}_n(\boldsymbol{k},\omega)$ are related to the photoemission setup, however, we use the assumption that $\mathcal{M}_n(\boldsymbol{k},\omega)$ is independent of time such that the matrix element is always determined in the equilibrium part of the TR-ARPES measurements. So, for the fits of the TR-ARPES data we account for the time dependent changes of FD distribution and spectral function by allowing a variation of T_e, ΔE_s and the self-energy through the scattering rate (Γ) and the gap parameter Δ. Data points acquired for $t < -100$ fs are described using a single optimized spectrum, as the system is in equilibrium. The parameters of this optimized spectrum are used as input for the fit of the TR-ARPES data points acquired at the remaining time delay points. We allow for a slight adjustment of the energy- and momentum-position of the bands to ensure consistency between measured and fitted spectra.

In Figs. S4(a)-(c) we show the TR-ARPES spectra, simulated spectra and the corresponding unsigned relative error ($|\ \varepsilon\ |$) at $t = -500$ fs, 60 fs and 2000 fs for the metallic phase ($T_s = 200$ K). The associated cumulative distribution of $|\ \varepsilon\ |$ is given in Figs. S4(d)-(f). As the actual intensity for the pixels above E_{F} is very small, irrespective of the simulation quality, the relative error for these pixels are high. We have therefore selected the energy range from -2.5 eV to E_{F} for our error analysis. All fitted pixels that fall below a margin set

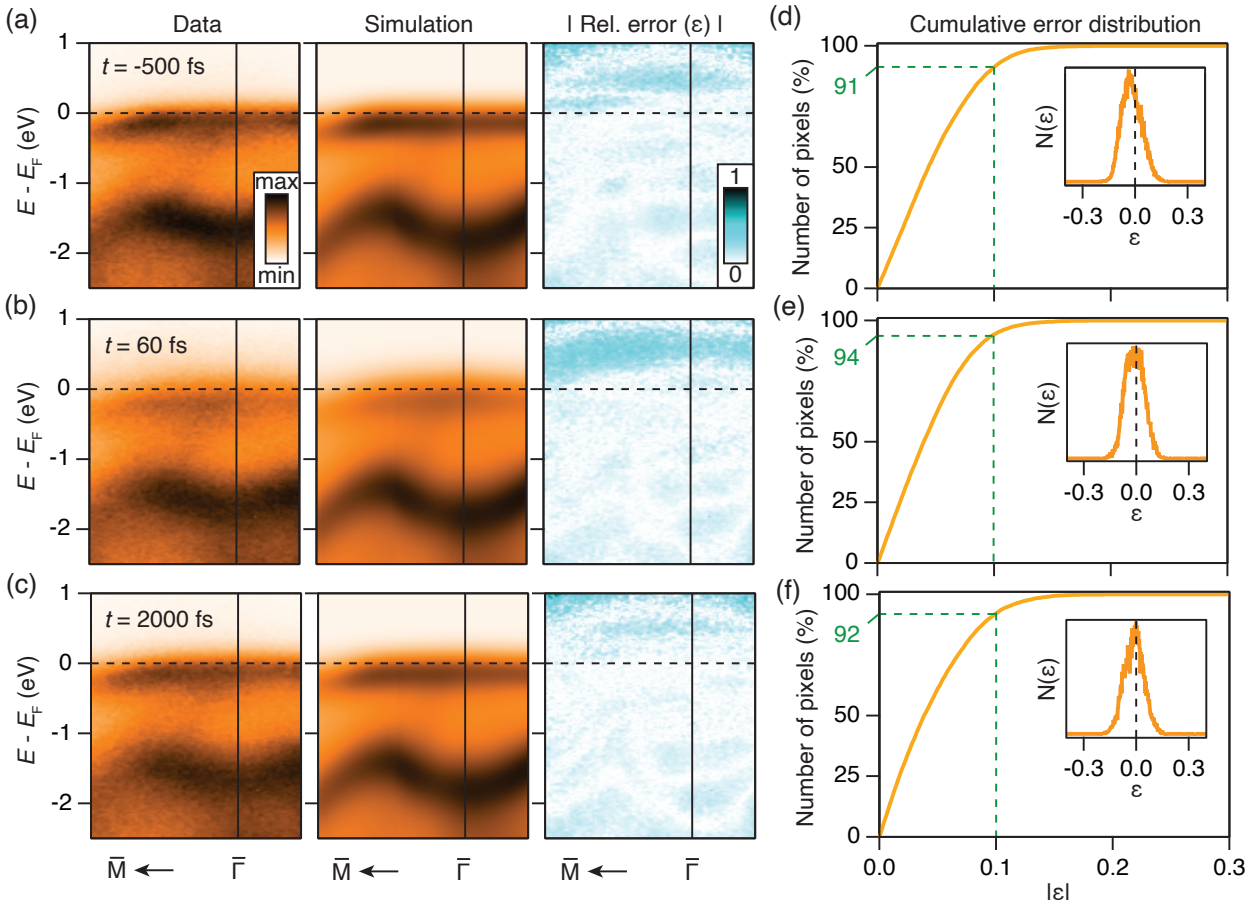

FIG. S4: Quality of simulation. (a)-(c) TR-ARPES specta for T_s = 200 K at the given time delays (left column). Simulated spectra and the corresponding unsigned relative errors (ε = (simulation-data)/data) are shown in the middle and right columns, respectively. (d)-(f) Cumulative distribution of $|\ \varepsilon\ |$ for the corresponding time-delays in the same row in (a)-(c) for the energy range -2.5 eV to E_F. The inserts present the distribution of ε. The green dashed lines in (d)-(f) correspond to $|\ \varepsilon\ |= 0.1$.

by $|\ \varepsilon\ |= 0.1$ are deemed as providing a satisfactory agreement between model and data. We find that this is the case for ≈92% of the pixels for all the three time delays. The symmetric distribution of the relative error (see inserts in Figs. S4(d)-(f)) with respect to ε = 0 shows the unbiased nature of our simulation.

In Figs. S5(a) and (b) we show the changes in the remaining fit parameters - scattering rate (Γ) associated with the V 3d band and the energy shift (ΔE_s) which accompany the parameters T_e and Δ shown in Fig. 3 of the main text. Figs. S5(c)-(f) present the intensity

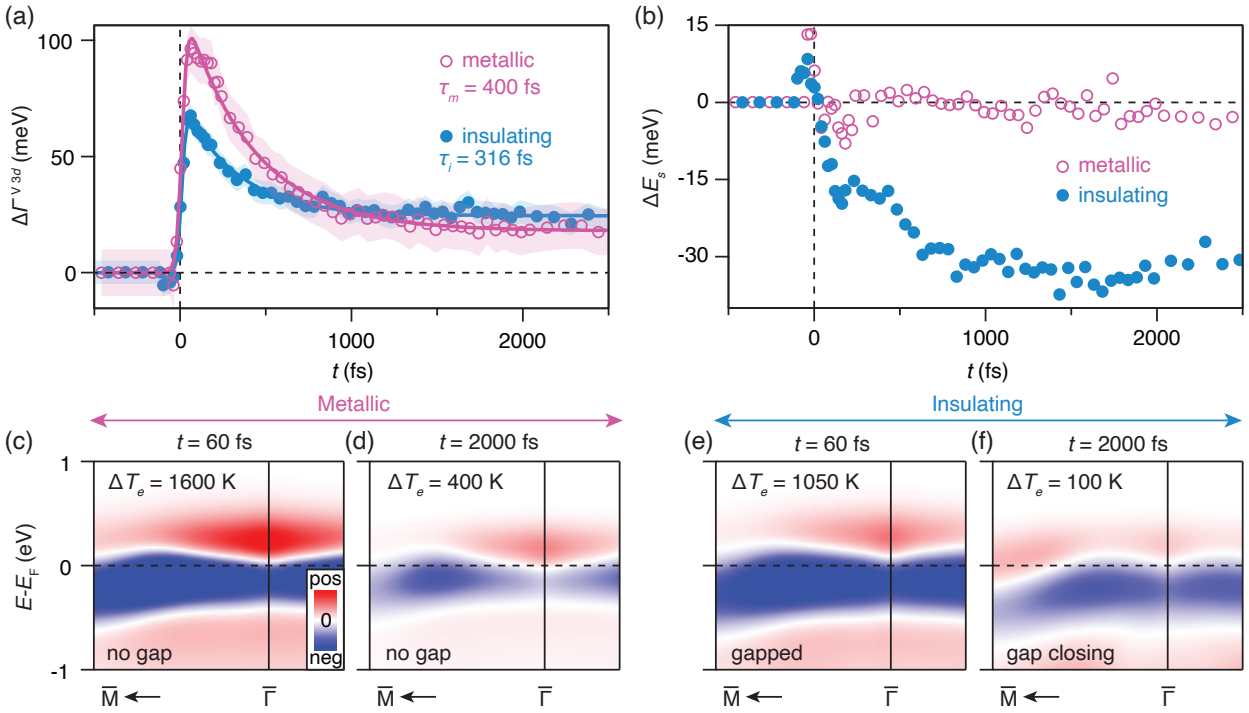

FIG. S5: Resulting parameters from fits of t-dependent photoemission intensity. (a) The change in the scattering rate (Γ) of V $3d$ states for both insulating (T_s = 88 K) and metallic (T_s = 200 K) phase. The solid curves show fits to a fast exponential rise followed by an exponential decay with the given time constants. (b) The corresponding rigid energy shift of the spectra, ΔE_s. (c)-(d) Difference between the fitted equilibrium spectra and the fitted spectra at the given time delays (60 fs and 2000 fs) for the metallic phase. (e)-(f) Corresponding difference spectra for the insulating phase.

difference calculated by subtracting the fitted equilibrium spectra from the fitted spectra at t = 60 fs and t = 2000 fs, which may be compared with the experimental results in Figs. 2(e) and (f) of the main manuscript.

In order to cross-check the optimization of Δ in the fit of the insulating phase data, we have generated difference spectra with values of Δ of 0, 30 and 60 meV, while keeping the rest of the parameters fixed to their optimized values. We pick the measurements at t = 60 fs and t = 2000 fs, shown in Fig. S6(a), as a check of the robustness of the fit in the dynamic and metastable phases of SL VSe_2. The corresponding simulated difference spectra are shown in Fig. S6(b). As Δ increases, the red contrast above E_F gets more pronounced

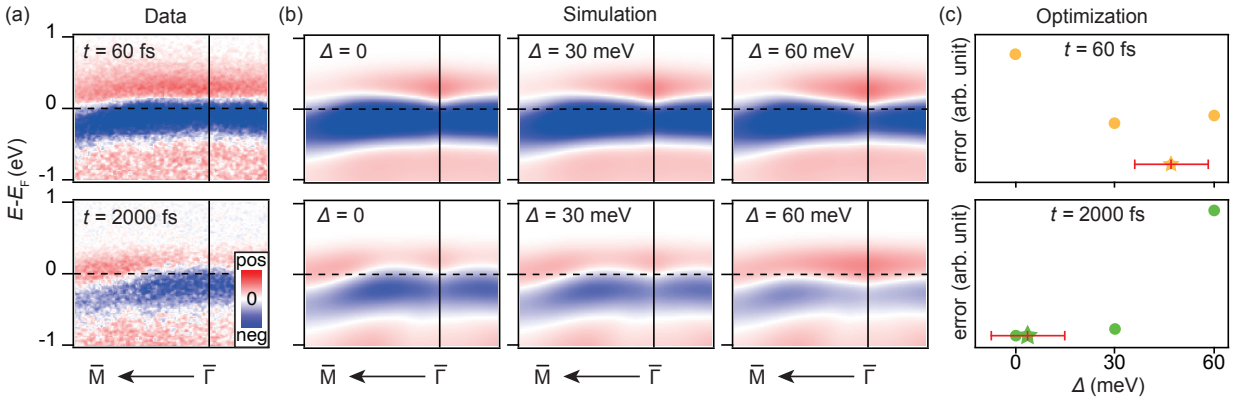

FIG. S6: Effect of gap parameter on difference spectra. (a) Measured difference spectra for the insulating sample at t = 60 fs and t = 2000 fs shown in top and bottom rows, respectively. (b) simulated difference spectra for changes of the gap parameter Δ given by 0, 30 and 60 meV with the remaining parameters kept fixed to their fitted values. (c) Absolute error in the fit for the given values of Δ at 60 and 2000 fs in the top and bottom panels, respectively. The "star" marker with the error bar indicates the value of Δ obtained from the fit where Δ is kept as a free parameter.

while the blue intensity below E_{F} shifts away from $\bar{\Gamma}$. These striking changes are caused by the change of the spectral function at finite Δ (see Fig. 1(f) in the main manuscript), asserting that even a small value of Δ can have a substantial impact on the time-dependent photoemission intensity around E_{F}. To quantify the error between data and simulation for the different values of Δ, we have calculated the squared difference between the data and simulation for each pixel and summed over the regions shown in Figs. S6(a)-(b). These values are plotted in Fig. S6(c) together with the value of Δ, resulting from the fit where Δ is kept as a free parameter (see "star" marker). The optimization shows that our fit yields a correct minimum for Δ within the error bar.

Supplementary Section 4: Reproducibility of intensity difference signals

We have performed consistency checks of the observed intensity difference by repeating the measurements discussed in the main manuscript for sample temperatures T_s of 88 K, 118 K, 166 K and 200 K and for two independent SL VSe_2 samples, verifying that the spectral

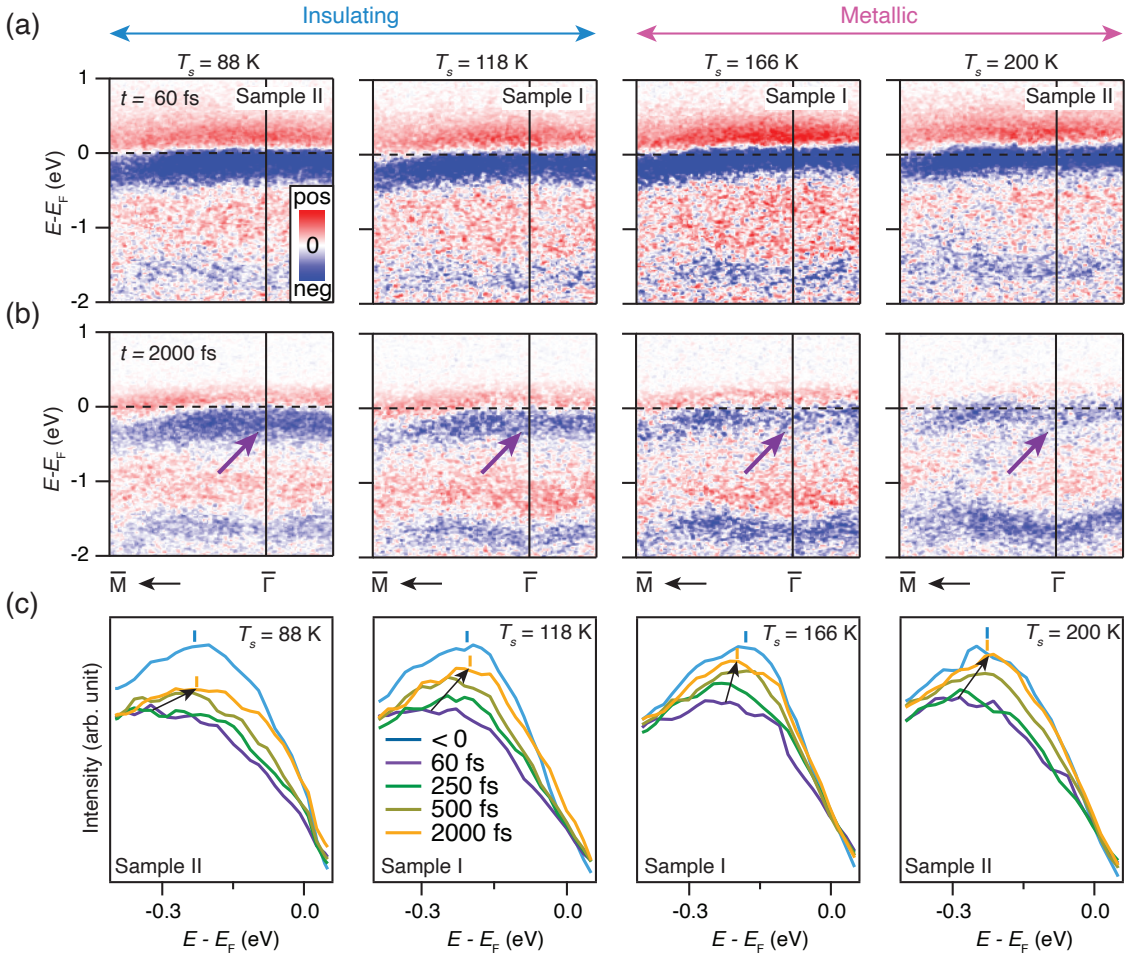

FIG. S7: Reproducibility of the response to optical excitation. (a) Difference spectra at t = 60 fs for sample temperature 88 K (sample II), 118 K (sample I), 166 K (sample I) and 200 K (sample II). (b) Corresponding difference spectra at t = 2000 fs. The purple arrows point to the (ω, k)-region of the spectra most strongly affected by the phase transition. (c) Corresponding EDCs around k_F at the given time delays. The blue and orange tick marks represent peak positions for t < 0 and t = 2000 fs, respectively. The black arrow indicates the change in peak position from t = 60 fs to t = 2000 fs.

signatures are robust for the two phases across T_c = 135 K. Figure S7 summarizes these results by presenting the corresponding intensity difference spectra and the EDCs around k_F at multiple time delays. The intensity difference is seen to exhibit identical shapes in the insulating and metallic phases as shown in Fig. 2(e)-(f) in the main manuscript. The EDCs present similar gap closing trends below 135 K as discussed in connection with Fig. 2(d) in the main manuscript.

Supplementary Section 5: Thickness and polymorphic structure of VSe_2

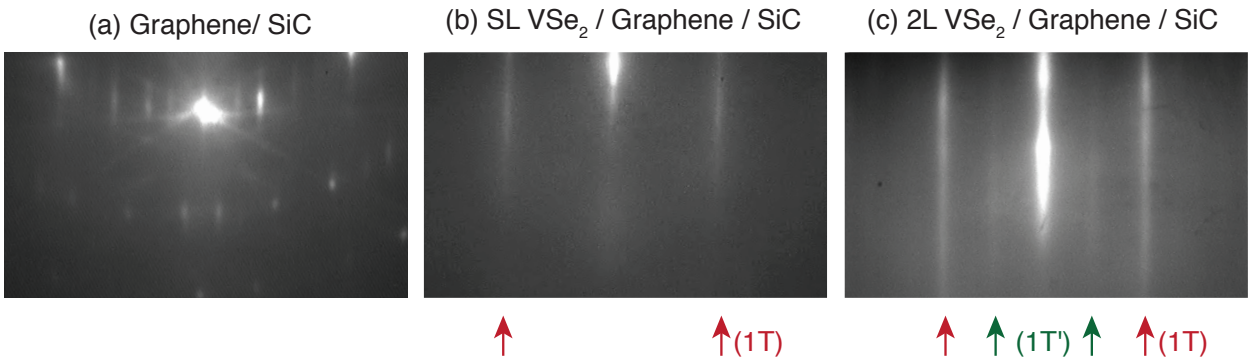

FIG. S8: Structure of VSe_2 samples. (a)-(c) In situ RHEED images for (a) graphene substrate, (b) SL VSe_2 and (c) bi-layer VSe_2 samples. The red arrows indicate stripes associated with the 1T phase of SL VSe_2. The green arrows indicate the 1T$'$ phase that occurs for multilayers of VSe_2.

Our SL VSe_2 samples were grown on bi-layer (BL) Graphene on SiC. Initially, the SiC substrates were outgassed at 650 $^\circ$C for a few hours and then annealed three times up to 1300°C for 2 min. The formation of BL graphene was verified by reflection high-energy electron diffraction (RHEED) and low-energy electron diffraction (LEED). High-purity V (99.8%) and Se (99.999%) were simultaneously evaporated while the substrate was kept at 250 $^\circ$C. The growth rate was fixed at 5 min per Se-V-Se layer. During the growth of VSe_2, the sample quality, structure and thickness were monitored in situ using RHEED. The RHEED images obtained from our graphene substrate, SL VSe_2 and bi-layer VSe_2 samples are shown in Fig. S8. The red and green arrows in panels (b) and (c) indicate stripes originating from 1T and 1T$'$ structures, respectively. The extra stripes in the case of the 1T$'$ polymorph are caused by an additional structural distortion, as observed in SL $ReSe_2$ [4] and multilayers of VSe_2 [5]. All our samples exhibit the RHEED pattern in Fig. S8(b), which is consistent with 1T SL VSe_2.

Supplementary Section 6: Determination of time resolution

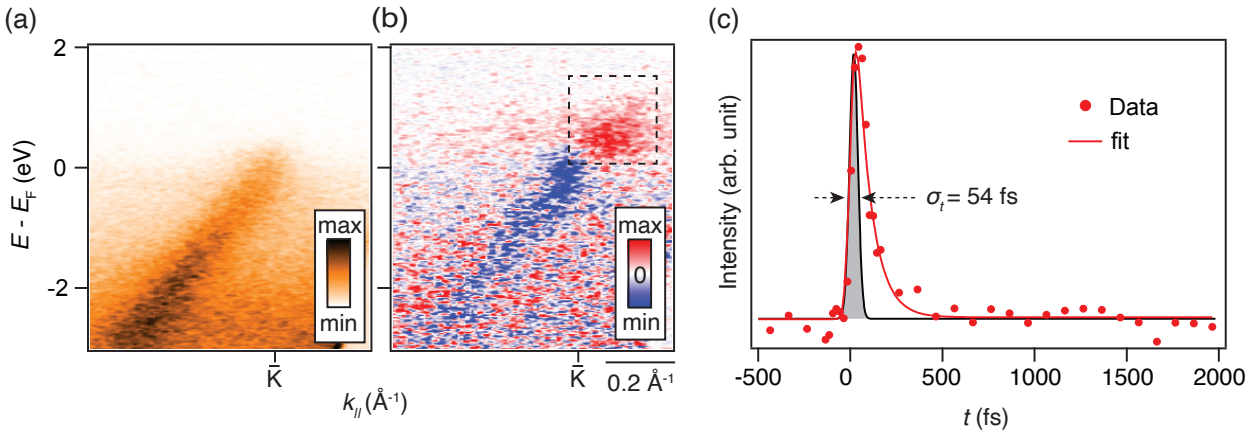

FIG. S9: Measurement of time-resolution on graphene substrate. (a) Photoemission intensity for graphene substrate for $t < 0$ around $\bar{\text{K}}$. (b) Intensity difference between a spectrum measured at $t = 60$ fs and the spectrum shown in (a). (c) Intensity difference integrated within the region marked by a dashed box in (b) as a function of time delay. The red curve is a fit to an exponential function convoluted with a Gaussian that accounts for the time resolution. The black curve represents the Gaussian with a FWHM of 54 fs.

We have performed TR-ARPES measurements on the graphene substrate in order to determine the time resolution of our experiment. A TR-ARPES spectrum for $t < 0$ and an intensity difference at $t = 60$ fs are presented in Figs. S9(a)-(b) around $\bar{\text{K}}$. The intensity difference integrated within the dashed black box in panel (b) is plotted as a function of time in panel (c), and a fit is performed with an exponential function convoluted with a Gaussian that accounts for the time resolution of the experiment. The full-width-at-half-maximum (FWHM) for the Gaussian is determined from the fit to be $\sigma_t = 54$ fs, which we use as an indication for the time resolution of the TR-ARPES experiment.

* address correspondence to: ulstrup@phys.au.dk

[1] M. Norman, M. Randeria, H. Ding, and J. Campuzano, Phys. Rev. B **57**, R11093 (1998).

[2] P. Chen, W. W. Pai, Y.-H. Chan, V. Madhavan, M. Y. Chou, S.-K. Mo, A.-V. Fedorov, and T.-C. Chiang, Phys. Rev. Lett. **121**, 196402 (2018).

[3] F. Andreatta, H. Rostami, A. G. Čabo, M. Bianchi, C. E. Sanders, D. Biswas, C. Cacho, A. J. H. Jones, R. T. Chapman, E. Springate, et al., Phys. Rev. B **99**, 165421 (2019).

[4] B. K. Choi, S. Ulstrup, S. M. Gunasekera, J. Kim, S. Y. Lim, L. Moreschini, J. S. Oh, S.-H. Chun, C. Jozwiak, A. Bostwick, et al., ACS Nano **14**, 7880 (2020).

[5] Y. Sun, T. Dai, Z. He, W. Zhou, P. Hu, S. Li, and S. Wu, Appl. Phys. Lett. **116**, 033101 (2020).